Journal of Asian Earth Sciences 50 (2012) 128–140

Contents lists available at SciVerse ScienceDirect

Journal of Asian Earth Sciences

journal homepage: www.elsevier.com/locate/jseaes

Origin and serpentinization of ultramafic rocks of Manipur Ophiolite Complex in the Indo-Myanmar subduction zone, Northeast India

P.S. Ningthoujam [a,*], C.S. Dubey [a], S. Guillot [b], A.-S. Fagion [b], D.P. Shukla [a]

[a] Department of Geology, Centre for Advanced Studies, University of Delhi, Delhi 110 007, India
[b] IsTerre, CNRS-OSUG, Université of Grenoble I, 1381 rue de la Piscine, 38041 Grenoble cedex 9, France

ARTICLE INFO

Article history:
Received 14 February 2011
Received in revised form 27 January 2012
Accepted 30 January 2012
Available online 25 February 2012

Keywords:
Indo-Myanmar Ranges
Manipur Ophiolite Complex
Serpentinite
Origin
Tectonics

ABSTRACT

The Manipur Ophiolite Complex (MOC) is part of the Manipur-Nagaland ophiolite belt (MNOB). The belt is exposed in the eastern margin of the Indo-Myanmar Ranges (IMRs), which formed by the collision between the India and Myanmar continental plates. Several contrasting views were put forward concerning the origin of the MNOB. The complex represents a dismembered ophiolite sequence with serpentinite as the largest litho-unit formed. Petrography and Raman spectroscopy of the serpentinite suggest that they are serpentinized ultramafic cumulate and peridotite. The serpentinization may have occurred at a condition of low pressure and low temperature metamorphism. Geochemical signatures of the rocks and spinel grains revealed that the protolith be an abyssal peridotite, derived from a less depleted fertile mantle melt at a MORB setting after low degree (10–15%) partial melting. The study concluded that the serpentinite may have been created at a slow-spreading ridge, rather than a supra-subduction-zone setting. These rocks were later obducted and incorporated into the IMR of Indo-Myanmar suture zone.

1. Introduction

The closure of the Tethyan oceanic realm during the Late Cretaceous and Early Tertiary preserved many ophiolite complexes within the Indo-Myanmar-Australia suture zones (Mitchell, 1981), including the MNOB in the Indo-Myanmar suture zone (Acharyya, 2007; Singh, 2008). The ophiolites, including serpentinite of the belt were derived from tectonic activities developed in the Tethyan oceanic lithosphere due to subduction of Indian plate below the Eurasian plate (Nandy, 1981; Oldham, 1883; Brunnschweiler, 1966).

The MOC is confined within the eastern sector of the IMRS (Vidyadharan et al., 1989; Singh, 2008). The complex is a dismembered ophiolite sequence with development of a mélange zone and an olistostromal plate margin (Evans, 1964; Vidyadharan et al., 1989). Well-preserved mantle sequences occur in the ophiolite belt (Acharyya, 1986; Ghose et al., 1986; Vidyadharan et al., 1989). However, the occurrence of serpentinite is observed as the most voluminous litho-tectonic unit in the complex. Pelagic sediments, pillow basalts, volcanic rocks, mafic dyke rocks and podiform chromitites are also exposed in minor in the complex. Rare occurrences of gabbros are observed in the study area.

Several contrasting views were put forward concerning the origin of the MNOB. One school of thought believed that the belt originated from multiple subduction processes of the Indian plate beneath the Eurasian Plate (Mitchell, 1993; Acharyya, 2007). Another school believed that the MNOB is rootless sub-horizontal bodies, which are westward-propagated nappes from the Eastern Belt Ophiolite of Myanmar (Sengupta et al., 1990; Acharyya et al., 1990). Another theory also believed that the belt originated in an Island Arc developed in the Tethyn Ocean (Bhattacharjee, 1991; Nandy, 2001). Furthermore, due to remote and inaccessible nature of the terrain, very less research work has been done in the area. An understanding of the origin of the MOC serpentinite is significant in evaluating the tectonic evolution of the subduction zone. A combination of petrological and geochemical studies of serpentinite can assist in determining the origin and geodynamic settings of serpentinization (Auzende et al., 2002; Hattori and Guillot, 2007; Saumur et al., 2010; Monsef et al., 2010). Raman spectroscopy can be used to study serpentine and the serpentinization processes (Kloprogge et al., 1999; Rinaudo et al., 2003; Auzende et al., 2004; Groppo et al., 2006). This paper details the origin and serpentinization of ultramafic rocks of the MOC through a combined effort of petrology and geochemical analysis. Origin and evolution of the MOC serpentinites, and in consequence, model of subduction of the Indian Plate and Myanmar Plate is discussed.

2. Geology and field setting

The MOC is located in the MNOB, which is confined within the eastern sector of the IMRs (Fig. 1). The belt constitutes a part of the

* Corresponding author. Tel.: +91 9990472324.
E-mail address: ningthoujamp@gmail.com (P.S. Ningthoujam).

1367-9120/$ - see front matter © 2012 Elsevier Ltd. All rights reserved.
doi:10.1016/j.jseaes.2012.01.004

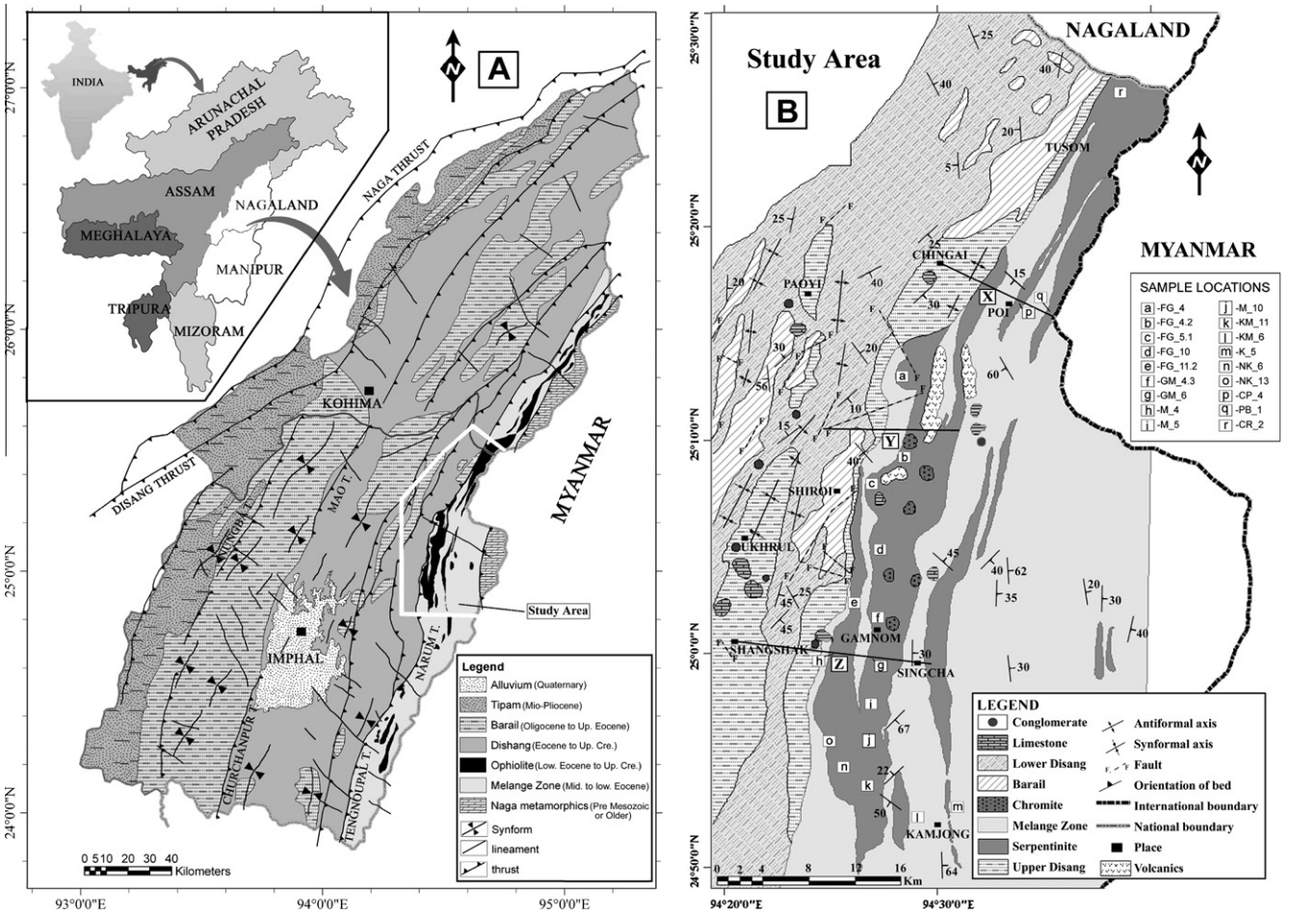

Fig. 1. (A) Geological map of the Manipur and Nagaland areas; White box show the location of the study area (Modified from GSI, M.N.C. DRG. No. 42/87; Soibam, 2006). (B) Geological map of the study area (Modified after Mitra et al., 1986; Vidyadharan et al., 1989).

Arakan-Yoma Fold Belt separating Northeastern India from Myanmar (Nandy, 1981). The belt forms a NNE–SSW trending linear tract with a length of about 200 km and has an average width of about 15 km. The IMR are mainly composed of the Late Cretaceous–Paleogene marine sedimentary rocks, unconformably overlying the Upper Triassic flysch-type sedimentary rocks and associated ophiolite rocks, thought to be the southern extension of the Indus-Yarlung Tsangpo suture zone (Mitchell, 1993).

The belt is bounded on the east by the Cenozoic sedimentary rocks of central lowland of Myanmar (Chattopadhyay et al., 1983) and to the west by a tectonic pile of the Tertiary overthrust known as the 'Schuppen Belt' (Evans, 1964) and Disang Group of Eocene. The belt has overthrusted the younger flysch sediments known as the Disang and the Barail (Fig. 1A). Bhattacharjee (1991) interpreted MNOB as slices of oceanic crust and upper mantle obducted onto the Indian continental margin. The linear tract consists of a complex mixture of igneous and sedimentary rocks representing oceanic and lithospheric assemblages. The belt is composed of highly dismembered composite zone of various rocks occurring as tectonic slices (Fig. 2). Principal rock types include dunite, harzburgite, lherzolite, wehrlite, pyroxenite and mafic volcanic rocks in association with oceanic pelagic sediments (Agarwal and Kacker, 1979; Ghose et al., 1986; Acharyya, 1986).

The MOC is wider in the northern side and gradually decreases in size towards the southern side and ultimately becomes discontinuous thereby giving patches of its existence in the south (Fig. 1A). A summary of the lithologies in the study area is given in Table 1. The Naga metamorphic of the Pre Mesozoic occurs as the oldest Group in the area (Brunnschweiler, 1966). They are found to occur on the eastern and northeastern fringes of the complex (Fig. 1A). The group consists of quartzite, crystalline limestone-marble, phyllite, mica schist, gneiss, sheared granite and minor serpentinite (Brunnschweiler, 1966; Roy and Kacker, 1980; Chattopadhyay et al., 1983). These rocks are occurring as klippen thrusted westward over the younger ophiolite belt of Lower to Upper Cretaceous (Fig. 2). The narrow strip of the main ophiolitic body is found to have a stretch of about 200 km in a NNE–SSW trend from Nagaland to Manipur (Fig. 1A.) as a continuous strip, and beyond it, the strip continues towards the south as discontinuous bodies and extended further into the Myanmar territory extending up to the Andaman-Nicober Isles. The ophiolite suite predominantly consists of well-preserved mantle sequence of peridotite with podiform chromitite along with mafic rocks and pelagic sediments (Singh, 2008). Vidyadharan et al. (1989) reported the occurrence of harzburgite, lherzolite, pyroxenite, gabbro, plagiogranite, volcanic rocks, agglomerates and oceanic pelagic sediments from the complex. However, in our detailed field work serpentinite are found to occur as the largest lithounit, they constitute much more than 90% of the exposure of the igneous ophiolitic rocks. The suite has thrusted contact with oceanic pelagic sediment (OPS) of the Middle to Lower Eocene. Some sporadic exposures of mafic rocks, including the extrusive pillow lavas and dyke rocks were observed in the complex (Fig. 1B). The Ophiolite complex is located within the Disang Group of Eocene to Upper Cretaceous (Fig. 1B). The term Disang was introduced by Mallet (1876) to describe a thick dark gray to black color splintery shale, interbedded

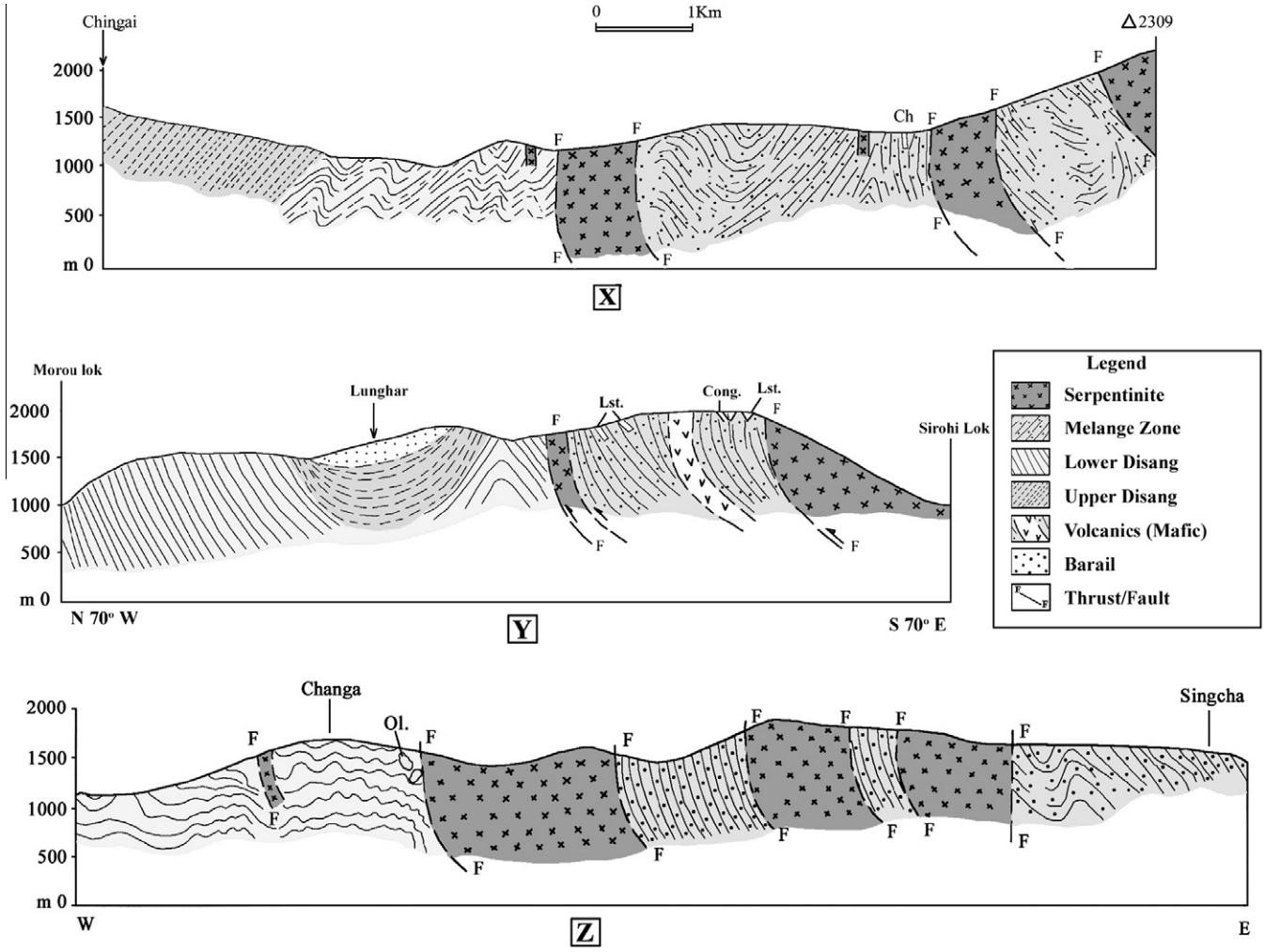

Fig. 2. Geological cross sections (A) From Chingai to Δ 2309 (B) Morou Lok to Sirohi Lok and (C) Changa to Singcha. (Modified after Vidyadharan et al., 1989).

Table 1
Geological succession of study area (Modified after Vidyadharan et al., 1989).

Group	Lithology	Age
Barail	Coarse, massive gritty, well-bedded sandstone showing current bedding, ripple mark, burrow, plant remains and coal streak.	Oligocene to Upper Eocene
Disang		
Upper	Patchy conglomerate with pebble of serpentine, chert, quartz; shale, siltstone, sandstone, rythmite, greywacke, olistostromal limestone, slice of ultramafic rock, pillow basalts, basic dyke, chert and OPS	Eocene to Lower Eocene
Lower	Dark splintery shale, siltstone, rythmite with greywacke, minor sandstone	
Oceanic Pelagic Sediment cover	Shale, thin sandstone, greywacke, intraformational conglomerate, red and green chert, clastic limestone, basic dykes and volcano sedimentary rocks	Middle to Lower Eocene
Ophiolite Suite	Serpentinized ultramafic rocks (peridotite), basic dykes, pillow basalt, amygdaloidal volcanics, podiform chromite	Lower Eocene to Upper Cretaceous
Metamorphic suite	Phyllitic schist, quartzite, micaceous quartzite, marble and quartz-chlorite-mica schist	Pre Mesozoic

with fine-grained sandstone and siltstone. The group also composed of conglomerate and olistostromal limestone. The Disang Group is underlain by coarse, massive gritty, well-bedded sandstone of the Barail Group of the Oligocene to Upper Eocene. The term Barail was coined by Evans (1932) for a sequence of alternating sandstone and shale (in varying proportions) in Assam, Nagaland and Manipur area.

In an idealized ophiolite belt, the proportion of peridotites and gabbros are similar (Winter, 2001), however in the MOC, absence of pyroxenite and gabbro was observed. Mafic rocks occur in the complex either as dykes or small exotic blocks within serpentinites and in pelagic sedimentary rocks. Small outcrops of pillow lava are also observed in the complex. Several patches of disseminated, massive and nodular, podiform chromitite deposits are observed

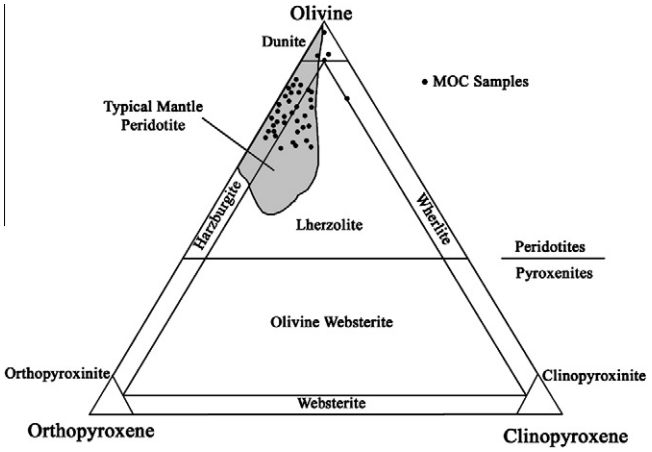

Fig. 3. Modal Analysis (point counting method) of ultramafic rocks (after Le Maitre et al., 2002).

in the complex. Few disseminated sulfide deposits were also reported (Vidyadharan et al., 1989).

Partially to fully hydrated peridotite, occur as the largest litho units in the study area, and constitute about 80–90% of the dismembered complex. In the field, serpentinites form ridges and undulating hills supported by scarce vegetation. The ultramafic bodies are always sandwiched in between pelagic shales (Fig. 2).They are frequently interceded by the Disang sediments and have an intrusive relationship with them (Fig. 2). The serpentinite of the complex is characterized by the presence of slicken sides, hobnail structures, conchoidal fractures, sheared masses with medium to a high degree of serpentinization. Serpentinite outcrops show a variable degree of shearing, brecciation and fracturing. According to the degrees of serpentinization, the ultramafic rocks of the area can be divided into two types. The first type is highly serpentinized with 80–90 degrees of serpentinization, with intense shearing along fractures developing slickensides. The second type is less serpentinized, with 50–60 degrees of serpentinization, and they exist as a fresh block embedded within highly hydrated ones. Point counting of the peridotite minerals inferred that they are mainly harzburgite and lherzolite with minor wehrlite as well as rare dunite (Ningthoujam, 2004) (Fig. 3).

3. Sampling and analytical methods

Serpentinite samples with various degrees of serpentinization were collected from different locations of the MOC (Fig. 1B). Detailed petrographic studies of the selected thin section slides were carried out at the Department of Geology, Centre for Advanced Studies, University of Delhi. Leica Workstation DMRX with the image analysis system was used to analyze the types of serpentine minerals present in ultramafic rocks.

Raman spectroscopy of samples was done at the Ecole Normale Superieure of Lyon, France with a Labram HR800 spectrometer and a visible laser source Spectra Physics® Ar + 2017, 514.5 nm. Two spectrum bands between 200 and 735 cm^{-1} for low frequencies and between 3500 and 3800 cm^{-1} for high frequencies (frequency corresponding to hydroxides) were harvested. The spectra was acquired between 30 s and one minute depending on the strength of the signal to minimize noise. The software PeakFit® was used for processing of spectra to determine the frequency of vibrations.

The Micro-X-ray Fluorescence (μXRF) of serpentinite samples was done using EDAX Eagle III XRF spectrometer at the IsTerre, CNRS-OSUG, Université of Grenoble, France. The device was equipped with a Rh anode and a polycapillary that focuses the X-ray beam down to an area of 50 μm width at half-maximum (FWHM). An EDX detector with resolution of 140 eV was used to measure the X-ray fluorescence. The instrument incorporates fast and simultaneous multi-element X-ray detection with the sensitivity to analyze from parts-per-million to 100% concentrations. Deconvolution of μXRF spectra was performed using the EDAX-integrated software Vision 32.

SEM EDS analysis of spinel grains was done at Department of Geology, University of Delhi using Zeiss M. A15. The device operates at 20 kV and equipped with an EDAX-DX4 energy dispersive spectrometer (EDS). Counting rate was kept close to 2200–2300 counts per second over the whole energy spectrum. Analytical precision was checked by repeated analyses and was better than 0.5% for major elements and better than 20% relative for minor elements (i.e., those ranging from 0.3 wt.% up to 3–5 wt.%).

4. Results

4.1. Petrography

4.1.1. Partially serpentinized peridotite

Most of the peridotites of MOC are highly serpentinized, but few are partially serpentinized. Relicts of harzburgite and lehrzolite frequently occur in the less serpentinized samples of the complex (Fig. 4A1). Wehrlite, dunite and pyroxenite are relatively infrequent as relict in the samples while websterite is absent. The presence of two generations of pyroxenes (orthopyroxene and clinopyroxene), with inclusion of olivine in both pyroxene grains are observed in most of the partially serpentinized samples. The samples contain secondary orthopyroxene replacing olivine. Some of the peridotites contain higher amounts of clinopyroxene relative to orthopyroxene because of metasomatic modification, suggesting that the initial peridotite was a depleted harzburgite to dunite (Coleman, 1971). Diopside grains are found in the rocks as the altered product of clinopyroxenes. Orthopyroxene is rarely preserved, being pseudomorphically replaced by either oriented lizardite/chrysotile, which are optically very similar, or very fine-grained diopside aggregates. At places, alteration of olivine and orthopyroxene relicts into greenish chlorite and talc are observed. Radiating cracks emerge out from the olivine relicts to the enclosing pyroxenes relicts, thereby suggesting that serpentinization are accompanied by an increase in volume.

4.1.2. Serpentinite

In the early stage of serpentinization, the textures of the original peridotites are still preserved. Relicts of olivine, orthopyroxene and clinopyroxene are visible in them (Fig. 4A1). Most of the serpentines are cut by late-stage serpentine veins, with a high variety of morphologies and textures that correspond to different mechanisms and conditions of formation. Several fine thread-like serpentine veins and veinlets occur in a crisscross pattern, exhibiting lensoidal (even curved tapering end), pinch and swell structure, sometimes branching like a braided river. In some samples, orthogonal and curvy veins are also noticed. Cracks and periphery of these minerals are being filled up with fine grained, flaky serpentine and generating primary veins (V1) (Fig. 4A1). Serpentinization advances in cracks and periphery of protolith. Primary veins (V1) replaced the protolith, and replacement texture is developed (Fig. 4A2). The serpentinization progresses and relicts of olivine and pyroxene start disappearing, keeping only the skeletal remains of the minerals. Mesh textures (Fig. 4B1) and bastite textures appeared in the rocks in place of pyroxene and olivine (Fig. 4C1). Afterward, the secondary veins (V2) develop in the rocks, intersecting the primary veins (V1) (Fig. 4B2). In the vein (V2), the serpentine minerals are fine-grained, fibrous. In the last stage of

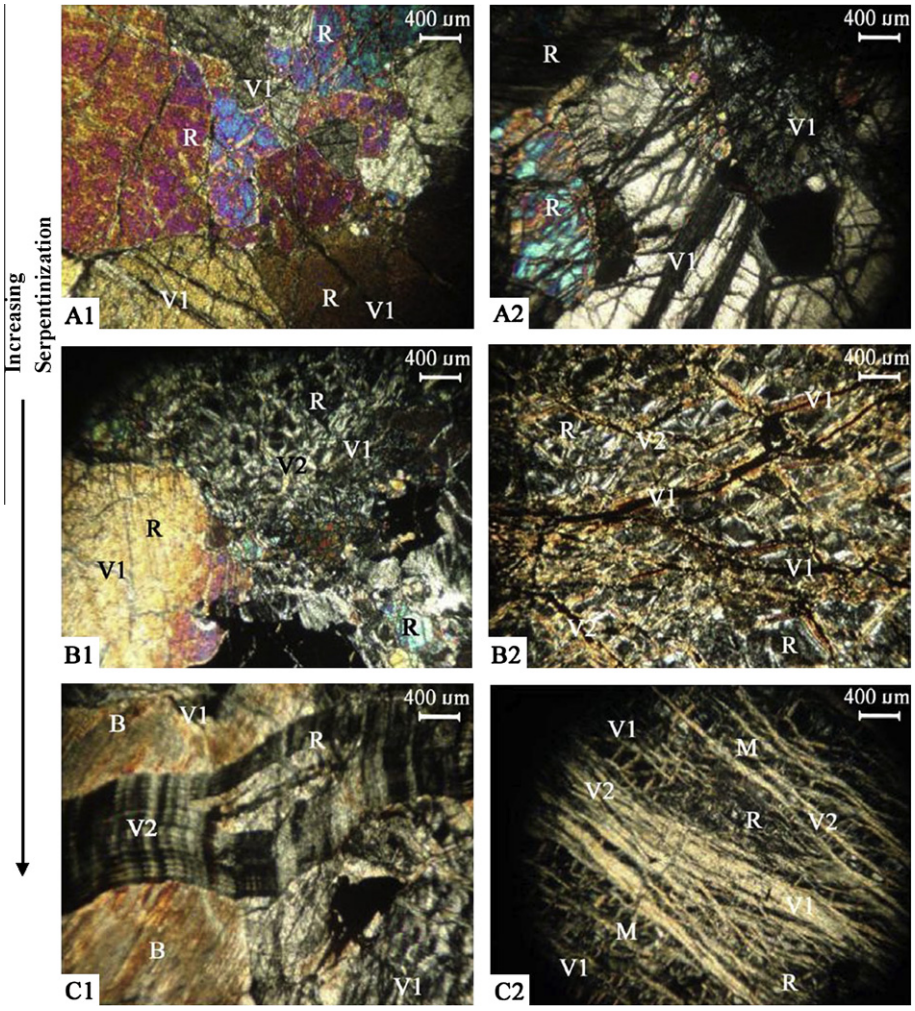

Fig. 4. Photomicrograph showing the increasing degree of serpentinization and development of veins in ultramafic rocks. R – relict of olivine and pyroxene, V1 – primary veins, V2 – secondary veins, B – bastite and M – mesh.

serpentinization, olivine and pyroxene grains are rare relicts in the rock and veins have developed and crisscross, developing a typical serpentine texture (Fig. 4 C2).

Well-fabricated bastite, mesh, window and hourglass textures are observed in the samples. The bastites formed by serpentinized orthopyroxene are found to occur as compact grains. They contain several cleavage planes (Fig. 4C2) and kink folds. The bastites emerged as pseudomorphs obliterating the original pyroxene cleavages. This shows that after most of the proportions of olivine have been serpentinized with considerable volume expansion, there must have been limited open spaces, by virtue of which volume expansion owing to serpentinization of pyroxene grains has been adjusted with the available accommodations between the cleavage planes. Most of the matrices in the samples contain flaky serpentines and show an olivine–serpentine mesh.

Lizardite occurs in serpentinite as fine-grained pseudomorphic, mesh and hourglass textures after olivine, enstatite and other minerals. They occur as flat, tabular crystals in the veins (mostly primary veins, V1) as well as the matrix but some lizardites in mesh rim occur as fibrous structure. The lizardite in mesh centers is fine grained and/or more poorly crystallized than that in mesh rims. Tabular lizardite also occurs as main minerals in bastite. Chrysotile occurs as fibrous, elongated crystals in secondary veins and as constituent minerals in mesh, hourglass textures. The chrysotile veins, cutting through the early formed serpentine mesh texture were observed in some sections. Chrysotile veins sometimes show small-scale displacement and bent in bastite textures indicating the effect of syn-serpentinization deformation. Bastites are often crossed by chrysotile veins and in some sample chrysotile completely replaces the lizardite bastite. In most of the studied samples, lizardite is found to occur as the most dominant serpentine variety in the form of veins as well as the matrix. Minor chrysotile is also found in most of the samples. Signature of antigorite and polygon serpentine were not observed in the study. For the confirmation of serpentine minerals present in the samples of MOC, we further intended for Raman Spectroscopy of the samples.

4.1.3. Spinel

We failed to observe garnet-bearing peridotite as reported elsewhere (e.g. Vidyadharan et al., 1989). Almost all the serpentinite samples are spinel-bearing varieties without garnet or plagioclase. Serpentine samples of MOC are associated with spinel and magnetite. Spinels are found to occur as fine to medium-grained, anhedral, irregular rounded and vermicular aggregates. They are found within the pseudomorph crystals of olivine and pyroxene. Magnetite occurs in a limited amount, as irregular fine to medium-grained crystals. Magnetites are commonly forming bands or dusty clusters of tiny opaque crystal rimming the altered primary phases. They occur in association with highly serpentinized materials thereby showing the relation of serpentinization and formation of magnetite. Al-spinels are more commonly present than

Cr-spinels in serpentinite samples of the MOC. SEM EDS analysis of spinel samples is discussed in following paragraph.

4.2. Raman spectroscopy

Raman spectroscopy is a simple and rapid technique that permits identification of mineral species without long and costly sample preparation. It has been an ideal technique to study the serpentinite, which often cannot be clearly characterized by optical microscopy and/or SEM–EDS (Groppo et al., 2006). Raman spectroscopy has been successfully used for differentiating the common phases of serpentine, chrysotile, antigorite and lizardite (Kloprogge et al., 1999; Lemaire et al., 1999; Rinaudo et al., 2003; Auzende et al., 2004; Groppo et al., 2006; Saumur et al., 2010). The Raman spectrometer measurements were made at several locations of rock thin sections of MOC, which were selected from petrographic studies. Selected spots in veins, as well as in the matrix were analyzed, and their respective peaks are studied. The results of the analysis are congruent with the pre-analyzed peaks by Auzende et al. (2004) and Groppo et al. (2006).

Auzende et al. (2004) distinguished four types of serpentine using Raman spectrometry, in various pressures (up to 10 GPa) in the high-(3550–3850 cm^{-1}) and low-(200–800 cm^{-1}) frequency ranges. Their studies resulted that, in the high-frequency domain (3550–3850 cm^{-1}), lizardite samples display two intense peaks at 3688 and 3703 cm^{-1} and chrysotile show a major peak at 3699 cm^{-1} with a shoulder at 3685 cm^{-1}. The two varieties also display a common very weak peak center around 3650 cm^{-1}. They also concluded that, in lower frequency, lizardite displays a very weak Raman peak at 240 cm^{-1} and in chrysotile it occurs at around 230 cm^{-1}. Groppo et al. (2006) have distinguished lizardite and chrysotile, on the basis of the SiO_4 tetrahedral bending modes. They concluded that the bending modes occur between 380 and 388 cm^{-1} in lizardite, while in chrysotile they occur at 390 to 394 cm^{-1}.

Presence of lizardite in serpentinite samples of the MOC was confirmed by the existence of two intense Raman peaks at 3688 cm^{-1}, 3703 cm^{-1} and a weak peak centered on 3650 cm^{-1}, in the high frequency domain (Fig. 5B). In the low frequency domain, presence of lizardite in the samples from the complex was confirmed by the incidence of Raman peak at 240 cm^{-1}, 380 to 385 cm^{-1}(Fig. 5A).

In high frequency, the existence of distinct Raman peak at 3699 cm^{-1}, with a shoulder at 3685 cm^{-1} and a weak peak centered on 3650 cm^{-1} confirmed the occurrence of chrysotile phases in the serpentinite samples of the complex (Fig. 6B). In low frequency, chrysotile occurrence in the serpentinite samples was confirmed by the existence of Raman peaks at around 230 cm^{-1}, 390 to 399 cm^{-1} (Fig. 6A). Peaks of lizardite were detected in a maximum number validating the presence of lizardite as the major serpentine variety in the complex. Peak of antigorite was not observed in the study.

4.3. Geochemistry

4.3.1. Serpentinite chemistry

4.3.1.1. Major and trace elements chemistry. The chemical compositions of serpentines from the MOC are presented in Table 2. However,

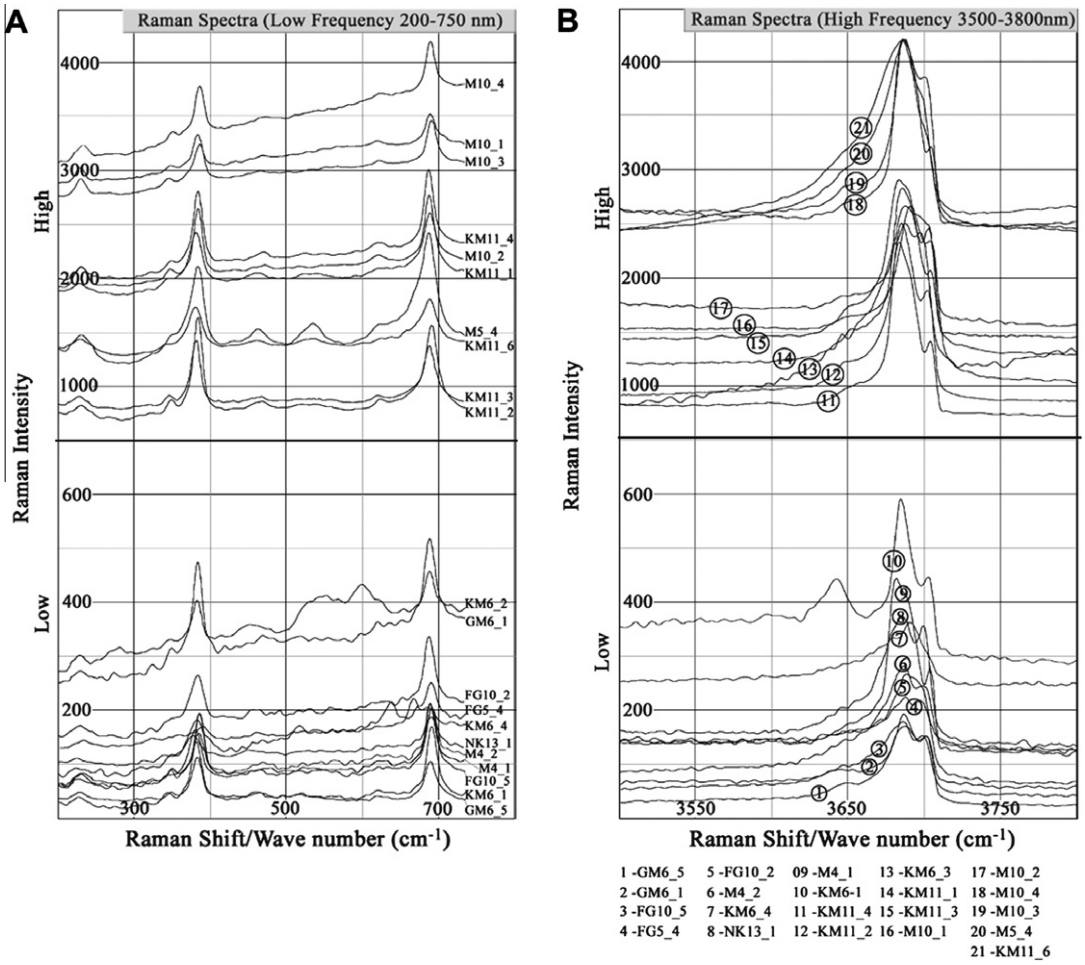

Fig. 5. Low frequency (A) and high frequency (B) Raman Spectra of lizardite.

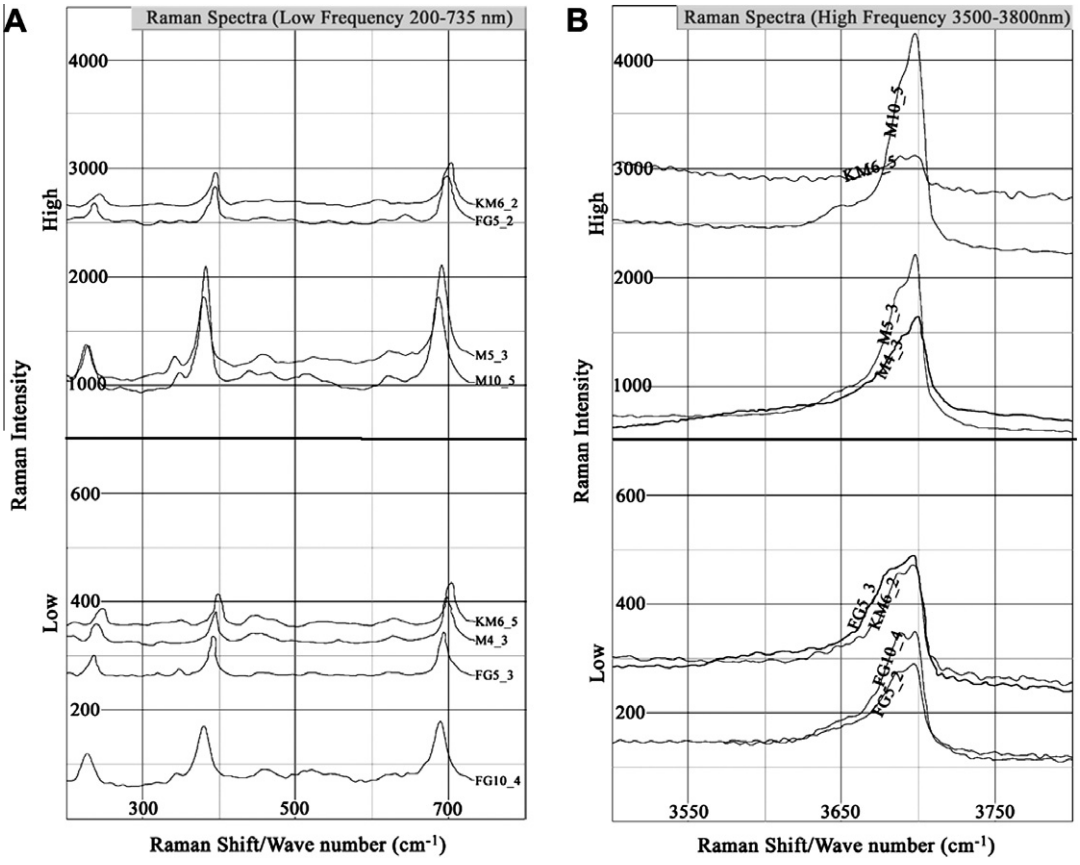

Fig. 6. Low frequency (A) and high frequency (B) Spectra of chrysotile.

Table 2
Chemical composition of serpentinite samples by micro-XRF.

Rocks (wt.%)	FG-11.2	PB-1	NK-13	NK-6	FG-10	FG-5.1	GM-6	KM-11	CP-4	CR-2	M-5	FG-4.2	GM-4.3	FG-4	K-5	KM-6	M-10	M-4
SiO_2	49.40	48.33	45.44	49.19	47.19	48.13	47.03	51.16	51.44	51.91	51.46	47.51	52.24	46.23	49.93	49.92	47.12	46.67
Al_2O_3	3.84	1.25	2.73	2.87	1.90	2.54	2.32	2.80	2.94	2.56	2.11	3.68	1.53	3.82	3.66	1.44	2.05	3.81
MgO	30.65	34.94	37.10	27.81	34.87	36.38	34.34	34.23	32.22	34.60	35.03	27.38	35.13	28.84	32.65	36.24	34.79	32.23
FeO (total)	11.13	12.64	10.87	12.10	12.30	9.44	12.27	6.55	9.55	7.91	8.54	13.79	9.00	11.91	8.29	8.81	12.12	8.42
MnO	0.75	0.40	0.27	2.20	0.16	0.23	0.28	-	0.12	0.18	0.29	0.50	0.21	0.41	0.30	-	0.23	0.20
Cr_2O_3	0.49	0.34	0.02	0.43	0.25	0.09	0.41	0.08	0.52	0.45	0.52	0.41	0.21	0.34	0.98	0.56	0.21	2.53
TiO_2	1.03	0.03	0.02	1.01	0.06	0.04	0.14	1.03	1.06	1.07	0.03	1.02	0.18	1.01	0.12	0.21	0.25	0.12
NiO	0.52	0.77	0.36	2.28	0.44	0.55	0.68	0.17	0.27	0.32	0.52	0.12	-	0.09	0.84	0.54	0.59	0.18
CaO	1.27	0.12	0.74	0.09	0.63	1.22	1.08	1.78	0.15	0.22	0.81	4.90	0.29	4.68	2.65	0.87	0.95	4.45
Na_2O	0.91	1.18	2.15	2.02	2.19	1.37	1.45	2.14	1.72	0.77	0.69	0.69	1.20	2.57	0.56	1.41	1.69	1.38
K_2O	–	–	0.03	–	–	–	–	0.06	–	–	–	–	–	–	–	–	–	–
Total	99.99	100	99.73	100	99.99	99.99	100	100	99.99	99.99	100	100	99.99	99.9	99.98	100	100	99.99
Coef.	2.533	2.561	2.571	2.583	2.569	2.529	2.570	2.480	2.496	2.472	2.490	2.591	2.484	2.556	2.509	2.511	2.567	2.552
Si	2.083	2.060	1.945	2.115	2.018	2.026	2.012	2.112	2.138	2.137	2.133	2.049	2.161	1.967	2.085	2.086	2.013	1.983
Ti	0.033	0.001	0.001	0.033	0.002	0.001	0.005	0.032	0.033	0.033	0.001	0.033	0.006	0.032	0.004	0.007	0.008	0.004
Al	0.191	0.063	0.138	0.145	0.096	0.126	0.117	0.136	0.144	0.124	0.103	0.187	0.075	0.192	0.180	0.071	0.103	0.191
Fe (2^+)	0.392	0.451	0.389	0.435	0.440	0.332	0.439	0.226	0.332	0.272	0.296	0.497	0.311	0.530	0.290	0.308	0.433	0.299
Mn	0.027	0.014	0.010	0.080	0.006	0.008	0.010	0.000	0.004	0.006	0.010	0.018	0.007	0.015	0.011	0.000	0.008	0.007
Mg	1.926	2.221	2.367	1.783	2.223	2.283	2.190	2.106	1.996	2.123	2.165	1.760	2.166	1.829	2.033	2.258	2.216	2.041
Ca	0.057	0.005	0.034	0.004	0.029	0.055	0.049	0.079	0.007	0.010	0.036	0.226	0.013	0.213	0.119	0.039	0.043	0.203
Na	0.074	0.098	0.178	0.168	0.182	0.112	0.120	0.171	0.139	0.061	0.055	0.058	0.096	0.212	0.045	0.114	0.140	0.114
K	0.000	0.000	0.002	0.000	0.000	0.000	0.000	0.003	0.000	0.000	0.000	0.000	0.000	0.000	0.000	0.000	0.000	0.000
Cr	0.016	0.011	0.001	0.015	0.008	0.003	0.014	0.003	0.017	0.015	0.017	0.014	0.007	0.011	0.032	0.019	0.007	0.085
Ni	0.018	0.026	0.012	0.079	0.015	0.019	0.023	0.006	0.009	0.011	0.017	0.004	0.000	0.003	0.028	0.018	0.020	0.006
Total	4.818	4.950	5.076	4.857	5.018	4.964	4.979	4.874	4.818	4.792	4.834	4.847	4.841	5.005	4.827	4.920	4.993	4.932
Cr#	0.079	0.154	0.005	0.091	0.081	0.023	0.106	0.019	0.106	0.105	0.142	0.070	0.084	0.056	0.152	0.207	0.064	0.308
Mg#	0.831	0.831	0.859	0.804	0.835	0.873	0.833	0.903	0.857	0.886	0.880	0.780	0.874	0.775	0.875	0.880	0.837	0.872

the analysis does not tell us about the exact composition of the minerals, as serpentinite is hydrous. Therefore, atoms per formula unit contents of serpentinite samples were calculated based on seven oxygen method. All the samples analyzed, have bulk rock compositions of typical serpentinized ultramafic rocks. Average Al_2O_3 value in the samples is 2.66 wt.%. The rocks have average 33.30 wt.% MgO.

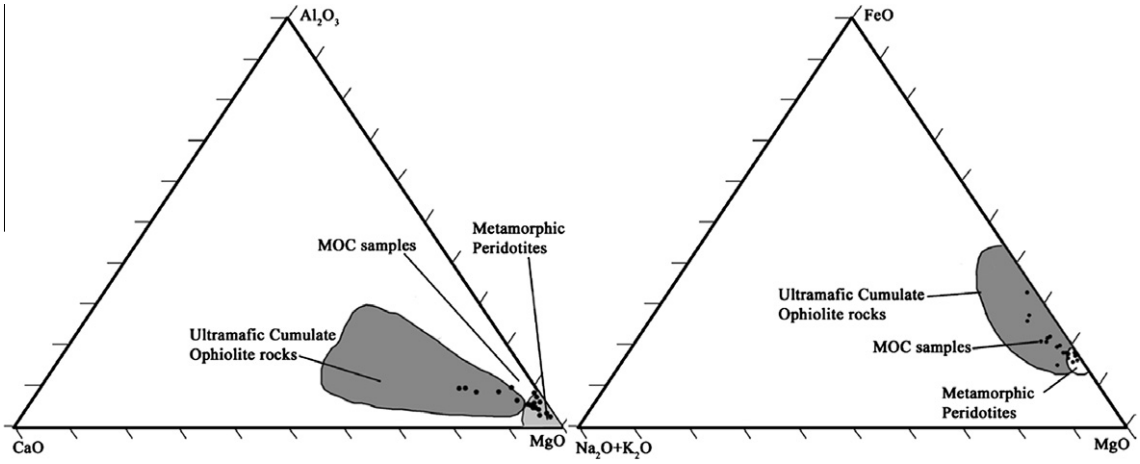

Fig. 7. AFM and ACM plots of ultramafic rocks. Fields of ultramafic cumulate and metamorphic peridotites are after Coleman (1977).

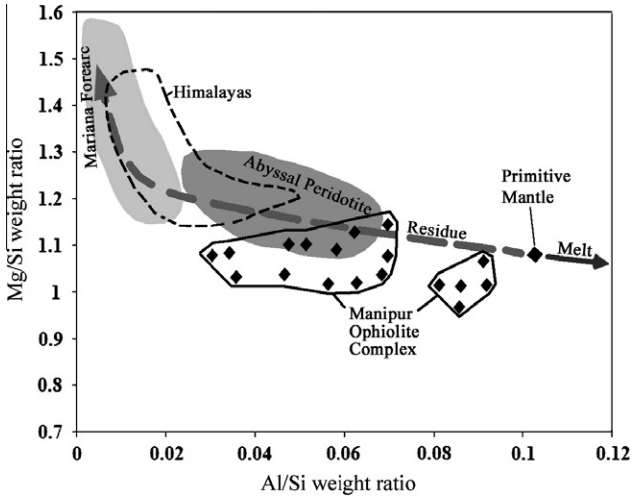

Fig. 8. Showing weight ratios of Mg/Si versus Al/Si serpentinite samples, in comparison with fields of peridotites of different origins. The diagram was based on the compositional variation of mantle peridotites compiled by Pearson et al. (2003) and Palme and O'Neill (2003), and abyssal peridotites by Niu (2004). The field of abyssal peridotite is defined by the 7th and 93rd percentile values of the Niu's data by Hattori and Guillot (2007). The expected compositional change of residual mantle peridotites during partial melting is shown with a thick gray arrow originating from the primitive mantle values (McDonough and Sun, 1995). Mariana forearc peridotites (light shaded area) are from Ishii et al. (1992). Himalayan samples residual peridotites are from Hattori and Guillot (2007). The compositional variation expected during partial melting is shown with gray arrow. (Modified after Saumur et al., 2010).

The samples contain an average value of 1.49 wt.% of CaO, 1.45 wt.% of Na_2O, and 0.37 wt.% of MnO. Average wt.% values of FeO and Cr_2O_3 in the samples are 10.31 and 0.51 respectively. The whole rock major elements, when plotted in a ACF and AFM ternary diagram shows that the serpentinized rocks of the MOC corresponded to a mixture of ultramafic cumulates and metamorphic peridotite (Fig. 7).

The samples from MOC have Al/Si value ranging from 0.03–0.10, with an average value of 0.06. The samples have 0.84–1.2 values of Mg/Si, with 1.02 average values. These values are lower than the primitive mantle values of Mg/Si and Al/Si, which are 1 and 1.3 respectively. The Mg/Si versus Al/Si value of most of the samples from MOC, when plotted in Mg/Si versus Al/Si binary graph, they clustered in two zones, one in a zone around abyssal peridotite and another in a zone nearly below primitive mantle value (Fig. 8).

Concentration of trace elements of serpentinite samples of MOC are given in Table 3. The samples are enriched in ultramafic transition elements (Ni = 1290–2670 ppm, and Cr = 557–1384 ppm). The high concentrations of Cr and Ni in the analyzed peridotites reflect their development from a depleted mantle peridotite source. Chondrite normalized rare earth element (REE) patterns of serpentinite samples of the MOC are given in Fig. 9. They have nearly similar and parallel REE pattern. They exhibit flat to slightly negative-sloped patterns with slight enrichment of LREE over HREE. REE patterns of most of the samples show positive Eu anomaly. Primitive Mantle (PM) normalized multi-element patterns for MOC serpentinite display nearly flat patterns like the REE (Fig. 10). Similar with the REE patterns, there is less variation in the abundances of most of the trace elements plotted in the spidergram. The prominent feature of the patterns is positive Eu anomalies in all the samples and zircon enrichment in some of the samples. It can be possibly related to plagioclase accumulation and/or due to impact of hydrothermal fluids. However, serpentinite samples of the MOC are plagioclase free. A possible interaction of Eu-enriched hydrothermal fluids with serpentinite increases the Eu content in the rocks (German et al., 1999; Douville et al., 2002; Paulick et al., 2006). The MOC serpentinite has relatively high alkalis, suggesting substantial hydrothermal fluid input during the formation of the rock. This explains the enrichment of Eu in the rocks.

4.3.2. Spinel chemistry

Mineral chemistry of selected primary spinel grains is presented in Table 4. The atoms per formula unit (APFU) contents of the samples were calculated after removal of the excess silica content, together with the magnesia and alumina contents in order to form ideal $Mg_3Si_2O_5(OH)_4$ serpentine. APFU of the samples is expressed based on four oxygens. The TiO_2 content of spinels varies between 0.03 and 0.21 wt.%, whereas the Al_2O_3 content of spinel varies between 46.01 and 53.132 wt.%. Binary diagram of TiO_2 wt.% vs. Al_2O_3 wt.% of spinel samples is shown in Fig. 11. The plot revealed that the serpentinite samples of MOC belong to MORB-type peridotite. The composition of spinels in serpentinite exhibits a similar range of Cr numbers (0.15–2.5) and Mg numbers (0.65–0.79) (Table 4). The binary plot of Cr vs. Mg numbers is shown in Fig. 12. The samples of MOC are clustered within and near the zone of abyssal peridotite.

5. Discussion

5.1. Source and origin of serpentinite

AFM and ACF ternary plots of the serpentinite samples of MOC inferred that the samples belong to a combined field of metamor-

Table 3
Trace element composition of serpentinite samples by ICP-MS.

Analyte	FG-11.2	PB-1	NK-13	NK-6	FG-10	FG-5.1	GM-6	CP-4	CR-2	M-5	KM-6
Trace element											
Cr	708.33	1108.89	1156.34	557.69	1163.67	1246.26	1198.70	655.70	1069.81	654.40	1384.00
Cu	115.71	78.88	99.92	51.63	73.05	79.51	43.07	24.20	86.49	90.84	42.02
Ga	19.84	14.62	13.99	13.41	14.00	13.35	12.46	6.76	14.60	23.86	13.97
Nb	0.26	0.34	0.62	0.33	0.31	1.00	0.30	0.65	0.97	0.37	0.28
Hf	1.55	0.10	0.10	0.09	0.55	0.60	0.04	0.04	0.53	2.26	0.04
Ni	1290.82	2176.19	2048.72	2618.62	2013.04	2119.11	2246.08	2670.02	2022.76	2175.99	1974.58
Pb	76.19	40.63	40.23	42.19	76.82	76.39	17.09	9.12	92.29	99.04	16.82
Rb	1.02	1.64	1.60	1.50	2.18	2.58	1.11	2.26	2.65	1.04	0.75
Sr	27.93	20.61	20.14	21.25	32.34	34.32	17.81	40.10	28.34	13.96	16.80
Th	0.49	0.22	0.23	0.22	0.35	0.39	0.12	0.10	0.39	0.56	0.09
U	0.30	0.16	0.13	0.17	0.25	0.25	0.09	0.04	0.27	0.46	0.13
V	476.79	83.23	82.81	49.02	93.58	114.94	72.92	77.07	89.89	445.29	59.55
Y	2.32	1.29	1.41	0.78	1.89	2.25	1.19	2.41	1.31	0.94	0.84
Zn	215.33	152.56	130.95	133.39	196.75	177.83	109.81	64.29	201.14	275.00	106.52
Zr	23.04	7.93	6.89	6.92	26.60	27.25	6.04	22.96	25.94	6.22	5.55
Ba	234.70	293.57	290.62	284.69	297.51	284.86	276.37	366.50	246.67	195.61	148.07
Co	37.10	124.74	118.13	150.61	114.20	128.58	126.50	141.75	114.70	47.96	115.97
REE											
La	1.01	0.69	0.98	0.66	1.07	1.15	0.61	1.18	1.15	0.66	0.57
Ce	1.72	1.25	1.57	1.14	1.96	2.04	0.90	2.44	2.17	1.12	0.99
Pr	0.17	0.13	0.15	0.13	0.21	0.24	0.13	0.26	0.24	0.13	0.12
Nd	0.79	0.55	0.54	0.48	0.81	0.88	0.50	1.04	1.01	0.45	0.50
Sm	0.13	0.07	0.10	0.11	0.07	0.09	0.20	0.09	0.13	0.19	0.16
Eu	0.41	0.46	0.45	0.45	0.47	0.49	0.43	0.55	0.45	0.46	0.32
Gd	0.30	0.14	0.25	0.18	0.21	0.36	0.22	0.52	0.48	0.21	0.20
Tb	0.30	0.14	0.25	0.18	0.21	0.36	0.22	0.52	0.48	0.21	0.10
Dy	0.39	0.18	0.18	0.15	0.25	0.32	0.15	0.36	0.26	0.15	0.15
Ho	0.06	0.03	0.03	0.03	0.04	0.05	0.03	0.06	0.05	0.03	0.03
Er	0.20	0.11	0.11	0.08	0.16	0.19	0.11	0.21	0.17	0.09	0.09
Tm	0.02	0.01	0.01	0.01	0.02	0.03	0.01	0.03	0.02	0.01	0.01
Yb	0.18	0.15	0.15	0.13	0.22	0.27	0.15	0.25	0.16	0.12	0.15
Lu	0.04	0.03	0.03	0.03	0.04	0.05	0.03	0.04	0.02	0.02	0.03

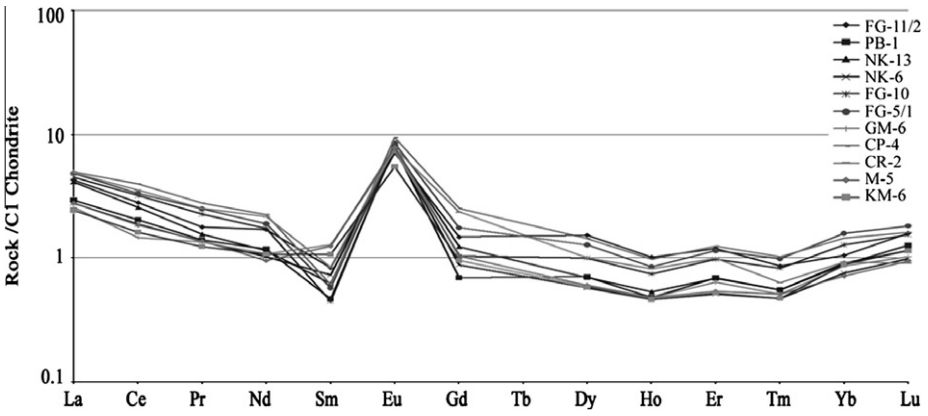

Fig. 9. C1 chondrite normalized rare earth element (REE) patterns of serpentinite. Normalize values after Sun and Mcdonough (1989).

phic peridotite and ultramafic cumulates. Higher average value of Al_2O_3 (2.66 wt.%) in the samples reflects a higher proportion of clinopyroxene phase than that of normal ophiolitic harzburgite and dunite, so the source of the samples is more fertile (Coleman, 1971). The nearly flat pattern of chondrite normalized REE, also indicates that the source of rocks is from a fertile mantle and have less variation in the degrees of partial melting. The slight enrichment of LREE in MOC serpentinite could be due to a hydrothermal metamorphic process of ocean water (~250–400 °C with up to 13 wt.% H_2O in serpentinites), during which the LREE could be mobile and added. (Niu, 2004). The samples are slightly enriched in LILE (Rb, Ba), which could be associated with seawater alteration or fluids produced by dehydration of obducted slab (Stolper and Newman, 1994; Keppler, 1996) or by interaction of LILE enriched hydrous fluids derived from the subducting slab (Stern et al., 1991).

The ratios of Mg/Si and Al/Si appear to provide definite parameters indicating a primary nature of the protoliths of the peridotite, as they did not change during the hydration and metamorphism of peridotite, and also that the ratios reflect those of anhydrous peridotite (Hattori and Guillot, 2007; Saumur et al., 2010). In Mg/Si versus Al/Si weight ratio diagram the serpentinite samples of MOC, clustered in two different zones. One clustered in a zone around abyssal peridotite and another in a zone virtually below primitive mantle value (Fig. 8). The decrease in Mg/Si weight ratio of some samples of MOC can be explained by enrichment of Si in Harzburgite (Coleman, 1977). Both Himalayas and MOC

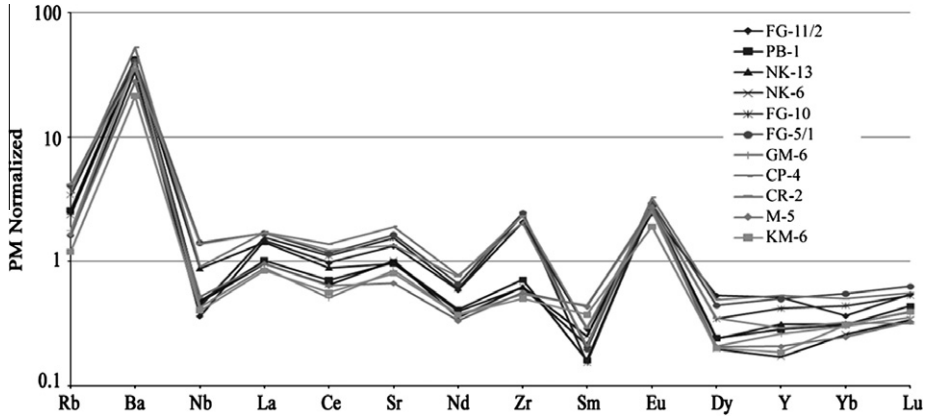

Fig. 10. Primitive Mantle (PM) normalized multi-element patterns of serpentinite. Normalize values after Sun and Mcdonough (1989).

Table 4
Chemical composition of spinel grains by SEM-EDS.

OXIDE (wt.%)	FG-11.2	PB-1	NK-13	NK-6	FG-10	FG-5.1	GM-6	KM-11	CP-4	CR-2	M-5	FG-4.2	GM-4.3	FG-4	K-5	KM-6	M-10
SiO_2	0.06	0.63	0.17	0.07	0.05	0.00	0.00	0.09	0.46	0.10	0.15	0.06	0.09	0.08	0.50	0.05	0.10
TiO_2	0.12	0.12	0.13	0.12	0.14	0.21	0.03	0.21	0.20	0.11	0.11	0.20	0.08	0.21	0.21	0.13	0.11
Al_2O_3	47.82	52.62	46.89	52.22	49.40	50.37	53.12	49.75	50.47	51.01	51.71	52.05	52.56	51.16	52.69	46.01	52.04
Cr_2O_3	13.08	16.65	23.47	15.10	22.14	18.91	15.38	19.81	14.78	17.18	17.86	19.13	20.30	17.93	17.96	19.23	16.00
Feo (total)	12.04	13.07	13.10	13.51	12.91	14.73	12.64	12.04	12.84	13.11	13.04	13.03	11.73	12.31	10.96	13.11	12.40
MnO	1.08	0.06	0.19	0.11	1.20	0.19	0.06	0.12	1.12	0.06	0.98	0.18	0.08	0.12	0.20	1.33	0.18
MgO	25.77	16.82	15.98	18.87	14.10	15.51	18.73	17.96	19.79	18.20	16.01	15.01	15.10	18.09	16.51	19.41	17.50
Cao	0.02	0.03	0.07	0.00	0.05	0.07	0.04	0.01	0.28	0.22	0.14	0.33	0.06	0.09	0.96	0.72	1.67
Total	99.99	100.00	100.00	100.00	99.99	99.99	100.00	99.99	99.94	99.99	100.00	99.99	100.00	99.99	99.99	99.99	100.00
Coef.	1.605	1.599	1.644	1.601	1.637	1.630	1.594	1.615	1.615	1.610	1.616	1.615	1.606	1.608	1.596	1.643	1.606
Si	0.002	0.017	0.005	0.002	0.001	0.000	0.000	0.002	0.012	0.003	0.004	0.002	0.002	0.002	0.013	0.001	0.003
Ti	0.002	0.002	0.003	0.002	0.003	0.004	0.001	0.004	0.004	0.002	0.002	0.004	0.002	0.004	0.004	0.003	0.002
Al	1.505	1.650	1.511	1.640	1.587	1.610	1.661	1.575	1.592	1.611	1.638	1.648	1.655	1.612	1.648	1.483	1.638
Fe(2^+)	0.269	0.291	0.300	0.301	0.294	0.334	0.280	0.270	0.287	0.294	0.293	0.293	0.262	0.275	0.243	0.300	0.277
Mn	0.024	0.001	0.004	0.002	0.028	0.004	0.001	0.003	0.025	0.001	0.022	0.004	0.002	0.003	0.004	0.031	0.004
Mg	1.026	0.667	0.651	0.750	0.573	0.627	0.741	0.719	0.790	0.727	0.642	0.601	0.601	0.721	0.653	0.792	0.697
Ca	0.001	0.001	0.002	0.000	0.001	0.002	0.001	0.000	0.008	0.006	0.004	0.009	0.002	0.003	0.027	0.021	0.048
Cr	0.276	0.350	0.507	0.318	0.477	0.406	0.323	0.421	0.313	0.364	0.380	0.406	0.429	0.379	0.377	0.416	0.338
Total	3.105	2.980	2.983	3.016	2.964	2.988	3.008	2.995	3.031	3.008	2.985	2.967	2.954	2.998	2.970	3.046	3.007
Mg#	0.792	0.696	0.685	0.713	0.661	0.652	0.725	0.727	0.733	0.712	0.686	0.673	0.697	0.724	0.729	0.725	0.716
Cr#	0.155	0.175	0.251	0.162	0.231	0.201	0.163	0.211	0.164	0.184	0.188	0.198	0.206	0.190	0.186	0.219	0.171

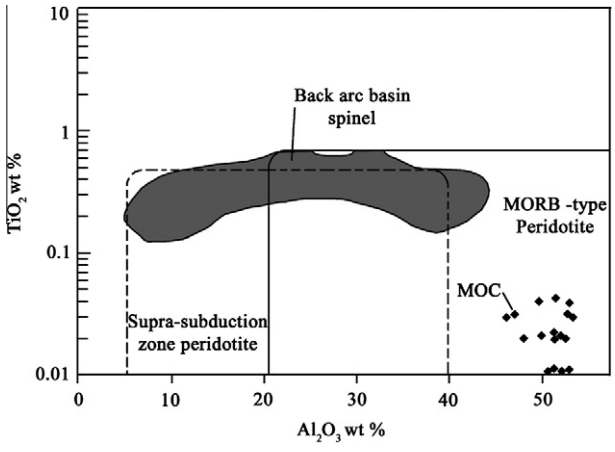

Fig. 11. TiO_2–Al_2O_3 plot of spinel of serpentinite (after Kamenetsky et al., 2001).

serpentinite were originated in Alpine-Himalayan Mesozoic Ophiolite belt. However, they are originated in different tectonic arcs. Therefore, there is a variation in their petrogenesis. The diagram indicates that most of the serpentinite samples of MOC are serpentinized from abyssal peridotite and among them few are derived from a fertile primitive mantle.

The composition of spinel in upper mantle tectonites provides further control on the petrogenesis of the ophiolite. The TiO_2 content (0.03–0.21) of MOC spinel is comparable with that of the mid-oceanic ridge tholeiites (TiO_2 = 0.16–0.85 wt.%) (Allen et al., 1988; Dick and Bullen, 1984). The Al_2O_3–TiO_2 variations of spinel of the MOC (Fig. 11) in comparison to modern-day tectonic settings depict that the spinels are plotted in the MORB-type peridotite. The Cr# of spinel in abyssal peridotite is a good indicator of the degree of partial melting for the mantle-derived spinel peridotite. Low Cr# spinel represents less depleted peridotite, whereas high Cr# spinel highlights more depleted peridotites (Dick and Bullen, 1984; Arai, 1994). The spinel grains present in serpentinite samples have low Cr numbers (0.15–2.5). Therefore, the samples originate from less depleted peridotite. This feature also reflects a low degree of partial melting and MORB extraction in the mid-ocean ridges (Allen et al., 1988; Kelemen et al., 1995). From the binary plot of Cr# (atomic ratio Cr/[Cr + Al^{3+}]) vs. Mg# (atomic ratio Mg/[Mg + Fe^{2+}]) for spinel grains (Fig. 12), it is clear that the samples showing a

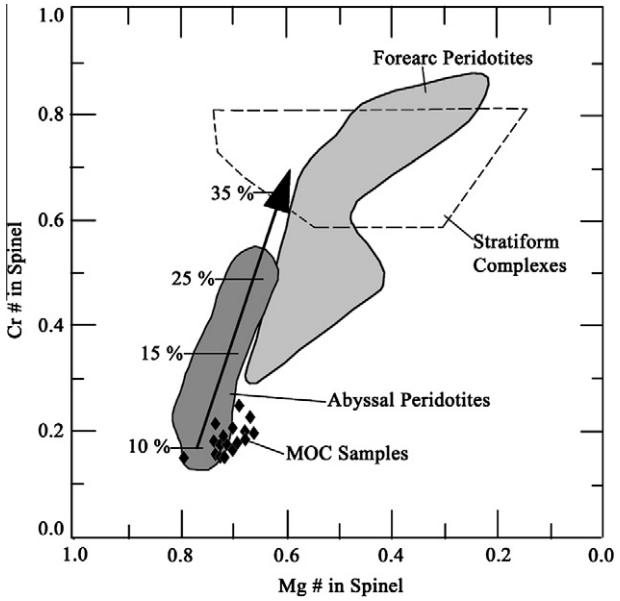

Fig. 12. Diagram of compositional variations in spinel. Cr# (= Cr/[Cr + Al] atomic ratio) vs. Mg# (=Mg/[Mg + Fe^{2+}] atomic ratio). Fields for spinels in abyssal peridotites is taken from a compilation by Dick and Bullen (1984). The field for fore-arc peridotites is from Ishii et al. (1992). The arrow represents the percentage of partial melting of the host peridotite (Hirose and Kawamoto, 1995).

tendency to be in the field of spinels from the abyssal peridotite. Based on calculations made by Hirose and Kawamoto (1995), the MOC serpentinite has 10–15% degrees of partial melting (Fig. 12).

Thus, from the above discussion, it can be concluded that the serpentinite samples of the MOC originated due to the low degree partial melting (10–15°) of a less depleted, fertile mantle melt in a spreading regime (MORB setting).

5.2. Geodynamic context of serpentinization

Petrography and Raman spectroscopy revealed that the serpentinite samples from the complex comprise of mainly lizardite, fewer chrysotiles and devoid of antigorite. Chrysotile and lizardite occur widely in serpentinites, commonly together, and correspond to inferred temperature conditions ranging from the surface up to perhaps as high as 400 °C; lizardite ~50–300 °C and chrysotile ~0–400 °C (Evans, 2004). Hilairet (2007) mentioned the possible existence of lizardite and chrysotile at low temperatures oceanic context to 200–400 °C. Bouchet (2008) suggest the occurrence of lizardite, chrysotile and antigorite at <200 °C, 200–300 °C and 300–600 °C respectively (Fig. 13). Therefore, serpentinite samples of the MOC might have been formed in low temperature oceanic ridge (200–350 °C) (Fig. 13).

Experimental studies have shown that among serpentine minerals, antigorite is the variety stable under high-pressure conditions (Bose and Ganguly, 1995; Wunder and Schreyer, 1997). Moreover, natural serpentinites sampled in high-grade terrains also display antigorite as the most abundant variety in the matrix (Mellini et al., 1987; Guillot et al., 2000; Auzende et al., 2002). Since the serpentinite samples of MOC are devoid of antigorite, there is no question of origin of the samples neither under a high-pressure condition nor high-grade oceanic terrains. Serpentinization in the MOC was mostly occurred at greenschist facies conditions or lower. Thus, we can conclude that serpentinite samples were originated in low-grade oceanic ridge (low temperature ~200–350 °C) under a low temperature–pressure condition (Fig. 13). Consequently, the serpentinites of the MOC can be related rather to a slow spreading zone than the subduction zone.

5.3. Tectonic evolution of MOC serpentinite

During the Early Cretaceous, the Australian and Antarctica in the Eastern Gondwanaland began to drift apart (Acharyya, 1998; Curray, 2005). Bhattacharjee (1991), based on radiolarian fossils (Nassellaria), assigned the age of the MOC chert as Early to Middle Cretaceous. Based on integrated coccolith-globotruncanid biostratigraphy of limestone blocks of the MOC, Chungkham and Jafar (1998) also suggest that initial rifting and creation of the Indo-Myanmar Ocean took place prior to the Late Santonian time. Geochemical analyses of ultramafic rocks and spinel grains inferred that the ultramafics of the MOC were originated due to the low degree partial melting (10–15°) of a less depleted, fertile mantle melt in a spreading regime (MORB setting). This tectonic setting can be related to the origin of ultramafic rocks of the MOC (Fig. 14).

During the Late Cretaceous, the Indian plate converged towards the Eurasian Plate and closing of the Neo-Tethys was started (Acharyya, 1998). Oceanic Ridges were building up on the weak rift zone developed in the Early Cretaceous (Fig. 14). The development of the ridges started plutonic and volcanic activities in the region. Ultramafic rocks from the oceanic crust as well as from the upper mantle were moved up along with the formation of the ridges. Mafic rocks and sediments were also raised up in the ridges.

In Late Cretaceous to Early Eocene, subduction of the Indian Plate beneath the Eurasian Plate was active. In the later part of Early Eocene, the subduction rate decreased at the suture due to the entry of a sea-mount into the subduction zone (Acharyya, 2007). However, the convergence of Plates was still continuing in the period. During this period, the Ocean basins along with the Ophiolite melange zone rose above the sea level (Fig. 14).

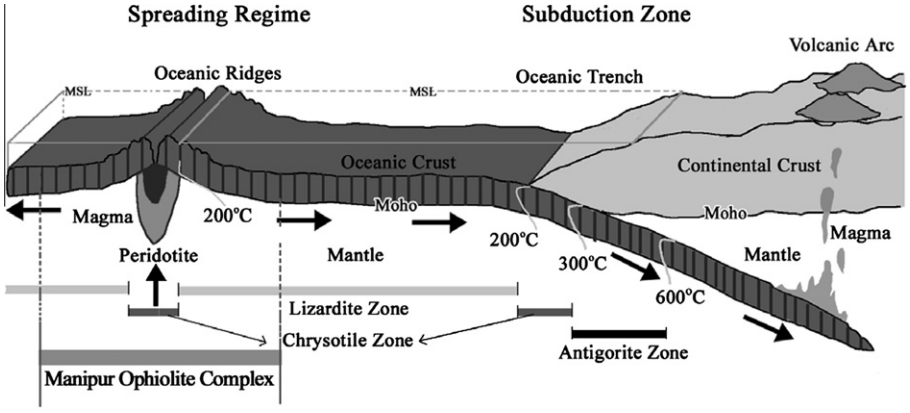

Fig. 13. Schematic diagram showing different origin zones of serpentine varieties and zone of formation of MOC serpentinites. (Temperature fields are after Bouchet, 2008).

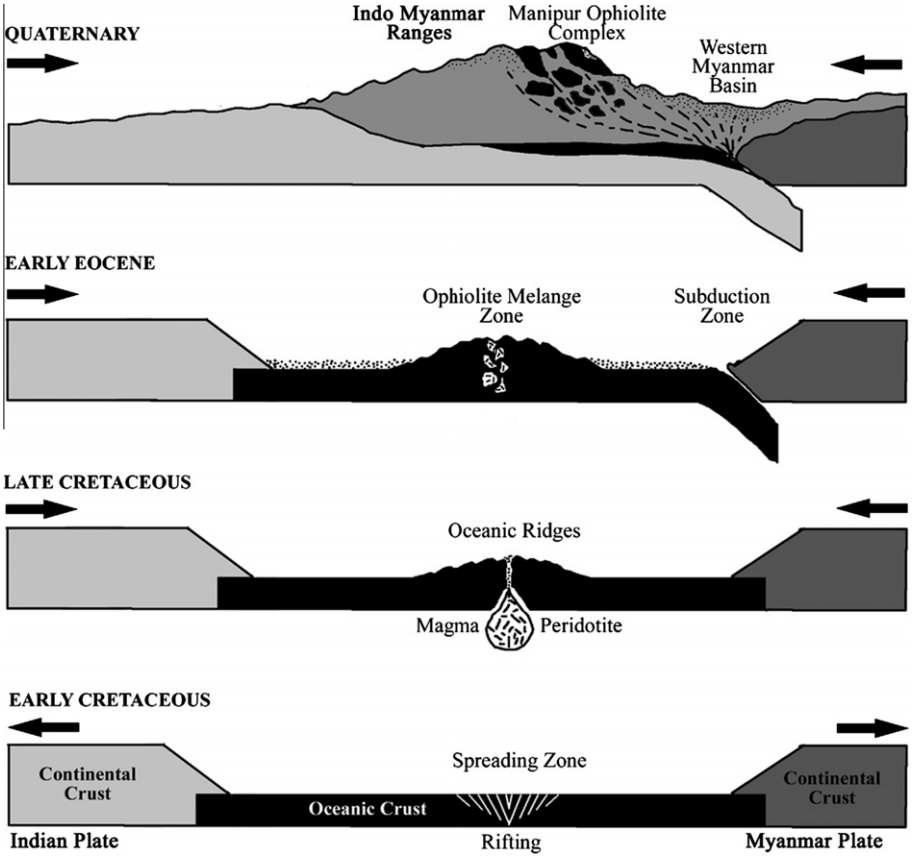

Fig. 14. Model of origin and serpentinization of ultramafic rocks of the MOC.

In the Miocene, the Sagaing Fault was developed in Western Myanmar (Mitchell, 1993) and consequently the magnitude of convergence due to subduction processes decreased. During the Quaternary, the IMR became stable and exposed in eastern boundary of the Indian Plate and the MOC exposed in the eastern flank of the IMR as an ophiolite-mélange zone (Fig. 14). Finally, present landscape of the IMR was developed and the MOC exposed in the eastern part of it as a part of the MNOB.

6. Conclusions

There is much confusion regarding the origin of the MNOB. This study focusing on petrology and geochemistry of the serpentinite component of the MOC helps clarify its tectonic setting. Our research work concluded that, even though the MOC serpentinites are exposed in the Indo-Myanmar subduction zone, they were originated at a spreading regime (MORB setting) due to the low degree partial melting (10–15°) of a less depleted, fertile mantle melt. Subsequently, the ultramafic rocks were serpentinized in a shallow ocean floor possibly at an ultra-slow to slow spreading regime. These rocks were later obducted and incorporated into the IMR of the Indo-Myanmar subduction zone.

Acknowledgements

Ningthoujam would like to thank UGC-CAS for providing fellowship for Ph. D. and R&D-DU for providing funds for this research work. We are indebted to the Prof. An Yin and Prof. Kéiko H. Hattori, for reviewing and giving constructive comments that greatly improved the manuscript. We are also thankful to Dr. Sandeep for providing facilities for ICP-MS. Thanks are due to Prof. Soibam Ibotombi, Manipur University for guiding us during our field work.

References

Acharyya, S.K., 1986. Tectono-stratigraphic history of Naga Hills Ophiolites. Geological Survey of India Memoirs 119, 94–103.
Acharyya, S.K., 1998. Break-up of the greater Indo-Australian continent and accretion of blocks framing South and East Asia. Journal of Geodynamics 26 (1), 149–170.
Acharyya, S.K., 2007. Collisional emplacement history of the Naga-Andaman ophiolites and the position of the eastern Indian suture. Journal of Asian Earth Sciences 29, 229–242.
Acharyya, S.K., Ray, K.K., Sengupta, S., 1990. Tectonics of ophiolite belt from Naga Hills and Andaman Islands, India. In: Naha, K., Ghosh, S.K., Mukhopadhyay, D. (Eds.), Structure and Tectonics, The Indian Scene. National Academy of Science India (Earth and Planetary Science), vol. 99. pp. 187–199.
Agarwal, O. P., Kacker, R.N., 1979. Nagaland ophiolite, India: A subduction zone ophiolite complex in Tethyan orogenic belt, In: Panayiotoau, A. (Ed.) Ophiolites. Geological Survey of Cyprus, pp. 454–461.
Allen, J.F., Sack, R.O., Batiza, R., 1988. Cr-spinels as petrogenetic indicators: MORB-type lavas from the Lamount seamount chain, eastern Pacific. American Mineralogist 73, 741–753.
Arai, S., 1994. Compositional variation of olivine – chromian spinel in Mg – rich magmas as a guide to their residual spinel peridotites. Journal of Volcanology and Geothermal Research 59, 279–293.
Auzende, A.-L., Devouard, B., Guillot, S., Daniel, I., Baronnet, A., Lardeaux, J.-M., 2002. Serpentinites from Central Cuba: petrology and HRTEM study. European Journal of Mineralogy 14, 905–914.
Auzende, A.-L., Daniel, I., Reynard, B., Lemaire, C., Guyot, F., 2004. High-pressure behavior of serpentine minerals: a Raman spectroscopic study. Physics Chemistry of Minerals 31, 269–277.
Bhattacharjee, C.C., 1991. The ophiolites of northeast India: a subduction zone ophiolite complex of the Indo-Burman orogenic belt. Tectonophysics 191, 213–222.
Bose, K., Ganguly, J., 1995. Experimental and theoretical studies of the stabilities of talc, antigorite and phase A at high pressures with applications to subduction processes. Earth and Planetary Science Letters 136, 109–121.
Bouchet, A., 2008. Characterization of serpentine present in the Oligocene conglomerates and Miocene syn-orogenic chains sub-alpine southern

(Western Alps): Identification of sources. Memory L3 Earth Sciences and planets, ENS Lyon.
Brunnschweiler, R.O., 1966. On the geology of the Indo-Burma Ranges. Geological Society of Australia 13, 127–194.
Chattopadhyay, B.M., Venkataraman, P., Roy, D.K., Ghose, S., Bhattacharya, S.S., 1983. Geology of Naga Hills Ophiolites. Records Geological Survey of India 113 (2), 59–115.
Chungkham, P., Jafar, S.A., 1998. Late Cretaceous (Santonian–Maastrichtian) integrated Coccolith–Globotruncanid biostratigraphy of pelagic limestone from the accretionary prism of Manipur, Northeastern India. Micropalaeontology 44, 68–83.
Coleman, R.G., 1971. Petrologic and geophysical nature of serpentinites. Geological Society of America, Bulletin 82 (4), 897–918.
Coleman, R.G., 1977. Ophiolites-Ancient Oceanic Lithosphere. Springer-Verlag, New York, Berlin.
Curray, J.R., 2005. Tectonics and history of the Andaman Sea region. Journal of Asian Earth Sciences 25, 187–232.
Dick, H.J.B., Bullen, T., 1984. Cr-spinel as a petrogenetic indicator in abyssal and alpine-type peridotites and spatially associated lavas. Contributions to Mineralogy and Petrology 86, 54–76.
Douville, E., Charlou, J.L., Oelkers, E.H., Bienvenu, P., Jove Colon, C.F., Donval, J.P., Fouquet, Y., Prieur, D., Appriou, P., 2002. The rainbow vent fluids (26o14'N, MAR): the influence of ultramafic rocks and phase separation on trace metal content in Mid-Atlantic Ridge hydrothermal fluids. Chemical Geology 184, 37–48.
Evans, P., 1932. Explanatory notes to accompany a table showing the tertiary succession in Assam: Trans. Mining and Geology International, India 27, 155–260.
Evans, P., 1964. The tectonic framework of Assam. Journal Geological Society of India 5, 80–96.
Evans, B., 2004. The serpentinite multisystem revisited: Chrysotile is metastable. International Geological Review 46, 479–506.
Geological Survey of India, 1987. Geological map of Manipur, M.N.C. DRG. No.42/87.
German, C.R., Hergt, J., Palmer, M.R., Edmond, J.M., 1999. Geochemistry of a hydrothermal sediment core from the OBS vent-field, 21°N East Pacific Rise. Chemical Geology 155 (1–2), 65–75.
Ghose, N.C., Agrawal, O.P., Singh, R.N., 1986. Geochemistry of the ophiolite belt of Nagaland, N.E. India, ophiolite and Indian plate margin. In: Ghose, N.C. (Ed.), Phanerozoic Ophiolites of India and Associated Mineral Resources. Suman Publication, Patna, pp. 241–293.
Groppo, C., Rinaudo, C., Cairo, S., Gastaldi, D., Compagnoni, R., 2006. Micro-Raman spectroscopy for a quick and reliable identification of serpentine minerals from ultramafics. European Journal of Mineralogy 18, 319–329.
Guillot, S., Hattori, K., de Sigoyer, J., 2000. Mantle wedge serpentinization and exhumation of eclogites: insights from eastern Ladhak northwest Himalaya. Geology 28, 199–202.
Hattori, K.H., Guillot, S., 2007. Geochemical character of serpentinites associated with high to ultrahigh pressure metamorphic rocks in the Alps, Cuba, and the Himalayas: Recycling of elements in subduction. Geochemistry Geophysics Geosystems 8, Q09010.
Hilairet, N., 2007. Role of serpentine in the dynamics of subduction zones: An Approach Experimental High Pressure and High Temperature, Ph. D. Thesis, Ecole Normale Superieure de Lyon Department of Earth Sciences – UMR 5570.
Hirose, K., Kawamoto, T., 1995. Hydrous partial melting of lherzolite at 1 Gpa: the effect of H_2O on the genesis of basaltic magmas. Earth and Planetary Science Letters 133, 463–473.
Ibotombi, Soibam, 2006. Relative plate motions in and around Manipur and its implications on the tectonics of Indo-Myanmar Ranges. Himalayan Geology 27, 111–122.
Ishii, T., Robinson, P. T., Maekawa, H., Fiske, R., 1992. Petrological studies of peridotites from diapiric serpentinite seamounts in the Izu- Ogasawara-Mariana Forearc, Leg 125. In: Proceedings for the ocean drilling program. Scientific Reports, Bonin/Mariana region, pp. 445–486.
Kamenetsky, V.S., Crawford, A.J., Meffre, S., 2001. Factors controlling chemistry of magmatic spinel: an empirical study of associated olivine, Cr-spinel and melt inclusions from primitive rocks. Journal of Petrology 42, 655–671.
Kelemen, P.B., Shimizu, N., Salters, V.J.M., 1995. Extraction of mid ocean-ridge basalt from the upwelling mantle by focused flow of melt in dunite channels. Nature 375, 747–753.
Keppler, H., 1996. Constraints from partitioning experiment on the composition of subduction-zone fluids. Nature 380, 237–240.
Kloprogge, J.T., Frost, R.L., Rintoul, L., 1999. Single crystal Raman microscopic study of the asbestos mineral chrysotile. Physical Chemistry Chemical Physics 1, 2559–2564.
Le Maitre, R.W., Streckeisen, A., Zanettin, B., Le Bas, M.J., Bonin, B., Bateman, P., Bellieni, G., Dudek, A., Efremova, S., Keller, J., Lamere, J., Sabine, P.A., Schmid, R., Sorensen, H., Woolley, A.R., 2002. Igneous rocks: a classification and glossary of terms, recommendations of the international union of geological sciences. In: Le Maitre, R.W. (Ed.), Sub-commission of the Systematics of Igneous Rocks. Cambridge University Press.
Lemaire, C., Guyot, F., Reynard, B., 1999. Vibrational spectroscopy (IR and Raman) of OH groups in chrysotile lizardite and antigorite. European Union of Geosciences 10, Strasbourg, pp. 654.
Mallet, F.R., 1876. On the coal fields of Naga hills bordering the Lakhimpur and sibsagar districts, Assam. Geological Survey of India, Memoir 12 (2), 166–363.
McDonough, W.F., Sun, S.S., 1995. The composition of the Earth. Chemical Geology 120, 223–254.
Mellini, M., Trommsdorff, V., Compagnoni, R., 1987. Antigorite polysomatism: behaviour during progressive metamorphism. Contributions to Mineralogy and Petrology 97, 147–155.
Mitchell, A.H.G., 1981. Phanerozoic plate boundaries in mainland SE Asia, the Himalayas and Tibet. Journal of the Geological Society of London 138, 109–122.
Mitchell, A.H.G., 1993. Cretaceous-Cenozoic tectonic events in the western Myanmar (Burma)-Assam region. Journal of the Geological Society of London 150, 1089–1102.
Mitra, N.D., Vidyadharan, K.T., Gour, M.P., Singh, S.K., Mishra, U.K., Khan, I.K., Ghosh, S., 1986. A note on Olitostromal deposits of Manipur. Record Geological Survey of India 114, 61–75.
Monsef, I., Rahgoshay, M., Mohajjel, M., Moghadam, S.H., 2010. Peridotites from the Khoy Ophiolitic Complex, NW Iran: Evidence of mantle dynamics in a supra-subduction-zone context. Journal of Asian Earth Science 38, 105–120.
Nandy, D.R., 1981. Tectonic pattern of northern India and adjoining region. Indian Journal of Earth Sciences 7 (1), 103–107.
Nandy, D.R., 2001. Geodynamics of Northeastern India and the Adjoining Regions, ACB Publications, P757 Block-A Lake Town, Kolkata, India.
Ningthoujam, 2004. Study of Mafic and Ultramafic rocks in and around Maku Lamkhai Road Section, Ukhrul distric, Manipur. M. Sc. Dissertation, Manipur University, pp. 44–45.
Niu, Y., 2004. Bulk-rock major and trace element compositions of abyssal peridotites: implications for mantle melting, melt extraction and post-melting processes beneath mid-ocean ridges. Journal of Petrology 45, 2423–2458.
Oldham, R.D., 1883. Report on the geology of parts of Manipur and Naga hills. Memoirs Geological Survey of India 19 (4), 216–226.
Palme, H., O'Neill, H.St.C., 2003. Cosmochemical estimates of mantle composition. In: Carlson, R.W. (Ed.), The mantle and core. Treatise on Geochemistry, vol. 2, pp. 1–28.
Paulick, H., Bach, W., Godard, M., De Hoog, J.C.M., Suhr, G., Harvey, J., 2006. Geochemistry of abyssal peridotites (Mid-Atlantic Ridge, 15o20'N, ODP Leg 209): Implication for fluid/rock interaction in slow spreading environments. Chemical Geology 234, 179–210.
Pearson, D.G., Canil, D., Shirey, S.B., 2003. Mantle samples included in volcanic rocks: Xenoliths and diamonds, In: Carlson, R.W. (Ed.), The mantle and core. Treatise on Geochemistry, vol. 2, pp. 171–275.
Rinaudo, C., Gastaldi, D., Belluso, E., 2003. Characterization of chrysotile, antigorite and lizardite by FT-Raman spectroscopy. Canadian Mineralogist 41, 883–890.
Roy, R.K., Kacker, R.N., 1980. Tectonic analysis of Naga Hills orogenic belt along eastern peri-Indian suture. Himalayan Geology 10, 374–402.
Saumur, B.-M., Hattori, H.K., Guillot, S., 2010. Contrasting origins of serpentinites in a subduction complex, northern Dominican Republic. Geological Society of America Bulletin 26530, 3.
Sengupta, S., Ray, K.K., Acharyya, S.K., de Smeth, J.B., 1990. Nature of Ophiolite occurrence along eastern margin of Indian plate and their tectonic significance. Geology 18, 439–442.
Singh, Athokpam Krishnakanta, 2008. PGE distribution in the ultramafic rocks and chromitites of the Manipur Ophiolite Complex, Indo-Myanmar Orogenic Belt, northeast India. Journal of Geological Society of India 72 (5), 649–660.
Stern, R.J., Morris, J., Bloomer, S.H., Hawkins, J.W., 1991. The source of the subduction component in convergent margin magmas: trace element and radiogenic evidence from Eocene boninites, Mariana forearc. Geochemica at Cosmochimica Acta 55, 1467–1481.
Stolper, E., Newman, S., 1994. The role of water in the petrogenesis of Mariana trough magmas. Earth and Planetary Science Letters 121, 293–325.
Sun, S.S., McDonough, W.F., 1989. Chemical and isotopic systematics of oceanic basalt: implications for mantle composition and processes. In: Saunders, A.D., Norry, M.J. (Eds.), Magmatism in the Ocean Basins, vol. 42. Geological Society of London Special Publication, pp. 13–345.
Vidyadharan, K.T., Joshi, A., Ghose, S., Gaur, M.P., Shukla, R., 1989. Manipur ophiolites: its geology, tectonic setting and metallogeny. In: Ghose, N.C. (Ed.), Phanerozoic Ophiolites of India and Associated Mineral Resources. Suman Publication, Patna, pp. 197–212.
Winter, J., 2001. An Introduction to Igneous and Metamorphic Petrology. Prentice Hall, New Jersey.
Wunder, B., Schreyer, W., 1997. Antigorite; high pressure stability in the system $MgO–SiO_2–H_2O$ (MSH). Lithos 41, 213–227.